Wong, P. T. T., Murphy, W. F., & Mantsch, H. H. (1982) *J. Chem. Phys. 76*, 5230.
Wong, P. T. T., Mantsch, H. H., & Snyder, R. G. (1983) *J. Chem. Phys. 79*, 2369.
Wong, P. T. T., Moffatt, D. J., & Baudais, F. L. (1985) *Appl. Spectrosc. 39*, 733.
Wong, P. T. T., Weng, S. F., & Mantsch, H. H. (1986) *J. Chem. Phys. 85*, 2315.

# Mixed-Chain Phosphatidylcholine Bilayers: Structure and Properties†

J. Mattai, P. K. Sripada, and G. G. Shipley*
*Departments of Medicine and Biochemistry, Biophysics Institute, Housman Medical Research Center, Boston University School of Medicine, Boston, Massachusetts 02118*
*Received December 11, 1986; Revised Manuscript Received February 11, 1987*

ABSTRACT: Calorimetric and X-ray diffraction data are reported for two series of saturated mixed-chain phosphatidylcholines (PCs), 18:0/*n*:0-PC and *n*:0/18:0-PC, where the *sn*-1 and *sn*-2 fatty acyl chains on the glycerol backbone are systematically varied by two methylene groups from 18:0 to 10:0 ($n$ = 18, 16, 14, 12, or 10). Fully hydrated PCs were annealed at −4 °C and their multilamellar dispersions characterized by differential scanning calorimetry and X-ray diffraction. All mixed-chain PCs form low-temperature "crystalline" bilayer phases following low-temperature incubation, except 18:0/10:0-PC. The subtransition temperature ($T_s$) shifts toward the main (chain melting) transition temperature ($T_m$) as the *sn*-1 or *sn*-2 fatty acyl chain is reduced in length; for the shorter chain PCs (18:0/12:0-PC, 12:0/18:0-PC, and 10:0/18:0-PC), $T_s$ is 1–2 °C greater than $T_m$, and the subtransition enthalpy ($\Delta H_s$) is much greater than for the longer acyl chain PCs. $T_m$ decreases with acyl chain length for both series of PCs except 18:0/10:0-PC, while for the positional isomers, *n*:0/18:0-PC and 18:0/*n*:0-PC, $T_m$ is higher for the isomer with the longer acyl chain in the *sn*-2 position of the glycerol backbone. The conversion from the crystalline bilayer $L_c$ phase to the liquid-crystalline $L_\alpha$ phase with melted hydrocarbon chains occurs through a series of phase changes which are chain length dependent. For example, 18:0/18:0-PC undergoes the phase changes $L_c \rightarrow L_\beta' \rightarrow P_\beta' \rightarrow L_\alpha$, while the shorter chain PC, 10:0/18:0-PC, is directly transformed from the $L_c$ phase to the $L_\alpha$ phase. However, normalized enthalpy and entropy data suggest that the overall thermodynamic change, $L_c \rightarrow L_\alpha$, is essentially chain length independent. On cooling, the conversion to the $L_c$ phases occurs via bilayer gel phases, $L_\beta'$, for the longer chain PCs or through triple-chain interdigitated bilayer gel phases, $L_\beta$*, for the shorter chain PC 18:0/12:0-PC and possibly 10:0/18:0-PC. Molecular models indicate that the bilayer gel phases for the more asymmetric PC series, 18:0/*n*:0-PC, must undergo progressive interdigitation with chain length reduction to maintain maximum chain–chain interaction. The $L_\beta$* phase of 18:0/10:0-PC is the most stable structure for this PC below $T_m$. The formation and stability of the triple-chain structures can be rationalized from molecular models.

The lipid composition of biological membranes is generally complex, with individual lipids differing from each other in a number of ways, viz., variation in the functional groups in the head-group region and variation in chain lengths at the *sn*-1 and *sn*-2 positions of the glycerol backbone, as well the degree of unsaturation of the acyl chains. With respect to the acyl chains, the tendency is for the *sn*-1 position to consist of saturated fatty acyl chains while the *sn*-2 position consists of unsaturated, branched, or short saturated chains.

Earlier investigations of model phospholipid systems have focused on phosphatidylcholines (PCs) containing identical acyl chains in the *sn*-1 and *sn*-2 positions of the glycerol backbone, and a number of studies have been reported using differential scanning calorimetry (DSC), X-ray diffraction, and spectroscopic and dilatometric methods (Chapman et al., 1967; Levine et al., 1968; Tardieu et al., 1973; Mabrey & Sturtevant, 1976; Janiak et al., 1976, 1979; Chen et al., 1980; Füldner, 1981; Ruocco & Shipley, 1982a,b; Nagle & Wilkinson, 1982; Cameron & Mantsch, 1982). With hydrated 1,2-dipalmitoyl-L-phosphatidylcholine (DPPC or 16:0/16:0-PC) as a classic example of a PC containing identical acyl chains, the following picture emerges for the structural changes accompanying the cooling of 16:0/16:0-PC from the liquid-crystalline bilayer phase ($L_\alpha$) (Chen et al., 1980; Füldner, 1981; Ruocco & Shipley, 1982a,b):

$$L_\alpha \leftrightarrow P_\beta' \leftrightarrow L_\beta' \underset{\text{fast}}{\overset{\text{slow}}{\rightleftharpoons}} L_c$$

The liquid-crystalline bilayer phase ($L_\alpha$) undergoes a transition to a "rippled" gel phase ($P_\beta'$) and then a further transition to a tilted chain, bilayer gel phase ($L_\beta'$). The $L_\beta'$ phase is metastable at low temperatures and undergoes a slow conversion to a "crystalline" bilayer phase ($L_c$) characterized by increased chain packing and dehydration (Chen et al., 1980; Füldner, 1981; Ruocco & Shipley, 1982a,b; Nagle & Wilkinson, 1982).

Recognizing the heterogeneity with respect to fatty acyl composition in biological membranes, more recent studies have concentrated on the physical properties of saturated mixed-chain PCs where the fatty acids attached at the *sn*-1 and *sn*-2 positions differ in chain length (Keough & Davis, 1979; Chen & Sturtevant, 1981; Stümpel et al., 1981, 1983; Mason et al., 1981a,b, 1983; Huang et al., 1983; Huang & Levin, 1983;

† This research was supported by Research Grant HL-26335 and Training Grant HL-07291 from the National Institutes of Health.

0006-2960/87/0426-3287$01.50/0 

McIntosh et al., 1984; Lewis et al, 1984; Tümmler et al., 1984; Hui et al., 1984; Serrallach et al., 1984). For most PCs, at least two transitions were observed corresponding to the pretransition and main transition. Generalizations have been made with regard to the main transition temperatures. For example, positional isomers with the longer chain in the *sn*-2 position on the glycerol backbone have higher transition temperatures and enthalpies (Keough & Davis, 1979). Such generalizations are not readily applicable to the low-temperature transitions, since the appearance of such transitions is a function of the thermal history of the sample.

Stümpel et al. (1983) have reported calorimetric and X-ray data on a number of identical-chain PCs, mixed-chain PCs, and $\beta$-phosphatidylcholines, and crystalline phases were observed for all lipids following low-temperature annealing. However, the chain length difference between the *sn*-1 and *sn*-2 positions was limited to four methylene groups. Structural studies of more asymmetric mixed-chain PCs were examined by McIntosh et al. (1984) and Hui et al. (1984), with attention focused primarily on the gel phases of these lipids. Recently, Serrallach et al. (1984) have made a detailed study of hydrated 14:0/16:0-PC and 16:0/14:0-PC. These positional isomers exhibit similar thermotropic and structural behavior. The overall structural changes can be summarized as follows:

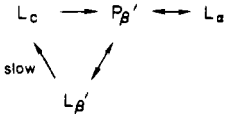


After long-term incubation at low temperatures, a crystalline bilayer phase, $L_c$, with an ordered chain packing mode is present; between the subtransition and main transition, the "rippled" gel phase, $P_{\beta'}$, is present while the liquid-crystalline $L_\alpha$ bilayer phase exists at high temperatures. On cooling, the $L_\alpha$ phase reverts back to the rippled phase $P_{\beta'}$, and then a new bilayer gel phase $L_{\beta'}$ is formed which converts to the $L_c$ phase with a functional dependence on time and temperature. This behavior is different from 16:0/16:0-PC, for which the $L_c$ phase on heating transforms to an $L_{\beta'}$ phase before forming the $P_{\beta'}$ phase (see above).

We have continued our calorimetric and X-ray diffraction studies of mixed-chain PCs by examining two extensive series where (a) the *sn*-1 fatty acyl chain is kept constant at 18:0 while the *sn*-2 chain is systematically decreased from 18:0 to 10:0 and (b) the *sn*-1 fatty acyl chain decreases from 18:0 to 10:0 while the *sn*-2 chain is fixed at 18:0. These two series of positional isomers, 18:0/*n*:0-PC and *n*:0/18:0-PC ($n$ = 18, 16, 14, 12, or 10), are examined with respect to their structure, metastability, and thermotropic properties.

## Materials and Methods

*PC Synthesis.* 18:0/18:0-PC was obtained in lyophilized form (>99% purity) from Avanti Polar Lipids (Birmingham, AL). Purity was checked by thin-layer chromatography using the solvent system $CHCl_3/CH_3OH/H_2O$ (65:25:4 v/v). The mixed-chain PCs 18:0/*n*:0-PC and *n*:0/18:0-PC ($n$ = 16, 14, 12, or 10) were synthesized according to the procedures of both Gupta et al. (1977) and Mason et al. (1981a) using the corresponding lysophosphatidylcholines (lysoPCs) (Avanti Polar Lipids, Birmingham, AL) and fatty acid anhydrides (Nu Chek Prep, Elysian, MN). The former procedure for the acylation of lysoPC involved the incubation of fatty acid anhydride (2.5 mol equiv relative to lysoPC compounds) in anhydrous chloroform in the presence of (dimethylamino)pyridine (Aldrich, Milwaukee, WI) as a base for 48–60 h at room temperature; the latter procedure used fatty acid anhydride (5 mol equiv) and pyrrolidinopyridine (Aldrich, Milwaukee, WI) as base, with incubation for 1–3 h at 35–40 °C. (Dimethylamino)-pyridine proved to be as effective a base as pyrrolidinopyridine. The products were purified by Rexyn I-300 treatment, followed by silicic acid column chromatography and crystallization from acetone/chloroform (95:5 v/v).

The isomeric purity of these lipids was checked by phospholipase $A_2$ cleavage of the fatty acid at the *sn*-2 position of the glycerol backbone followed by gas–liquid chromatography (GLC) analysis of the methyl esters of the acids according to Morrison and Smith (1964). Both synthetic procedures gave similar results with respect to acyl group migration (<5%) when the longer fatty acyl chains ($n$ = 18, 16, or 14) are on either the *sn*-1 or the *sn*-2 position of the glycerol backbone. However, for the more asymmetric PCs, 18:0/12:0-PC and 18:0/10:0-PC, synthesized according to the method of Gupta et al. (1977), acyl migration was found to be 8–10%. These PCs were therefore synthesized according to the method of Mason et al. (1981a), resulting in <5% acyl migration, i.e., similar to that obtained for the other mixed-chain PCs.

*Differential Scanning Calorimetry (DSC).* Samples (1–3 mg) of PC were weighed into stainless-steel DSC pans, and approximately 90% by weight of distilled deionized water was added by using a Hamilton syringe. The pans were hermetically sealed, and hydrated multilamellar dispersions were formed by heating and cooling the sample several times above and below the main transition temperature of the lipid in the calorimeter. Samples were removed and stored at −4 °C until use.

Calorimetric measurements were made with a Perkin-Elmer (Norwalk, CT) DSC-2 differential scanning calorimeter at a heating and cooling rate of 5 °C/min. The peak maximum in the plot of excess heat capacity vs. temperature was taken as the transition temperature, while the area under the peak, calibrated with a gallium standard, gave the transition enthalpy. DSC measurements of dilute dispersions (0.04% PC) of the mixed-chain PCs were also made with a Microcal MC-2 scanning calorimeter (Microcal, Amherst, MA) at a heating rate of 1 °C/min. Transition temperatures and enthalpies for the pretransition and main transition were in very good agreement with values obtained by using the DSC-2 scanning calorimeter.

*X-ray Diffraction.* For X-ray diffraction, hydrated multilamellar dispersions were prepared by adding weighed amounts of PCs directly into 1-mm quartz capillary tubes followed by centrifugation to ensure that the lipids reached the bottom of the capillary. Distilled, deionized water was added (50 wt %); the tubes were centrifuged, reweighed, and then flame sealed. The sealed tubes were centrifuged several times above the transition temperature of the lipids, with regular inversions to ensure homogeneous mixing, and then stored at −4 °C until use.

X-ray diffraction patterns were recorded by using photographic film and nickel-filtered Cu $K_\alpha$ radiation ($\lambda$ = 1.5418 Å) from an Elliott GX-6 rotating anode generator (Elliott Automation, Borehamwood, U.K.). The X-rays were focused into a point source using cameras with toroidal (Elliott, 1965) and double-mirror (Franks, 1958) optics.

## Results

### *Differential Scanning Calorimetry (DSC) of Hydrated (~90 wt % Water) Saturated Mixed-Chain PCs, 18:0/n:0-PC and n:0/18:0-PC (n = 18, 16, 14, 12, or 10)*

*18:0/n:0-PC.* Fully hydrated samples of mixed-chain PCs were stored for a minimum of 2 weeks, and in some cases

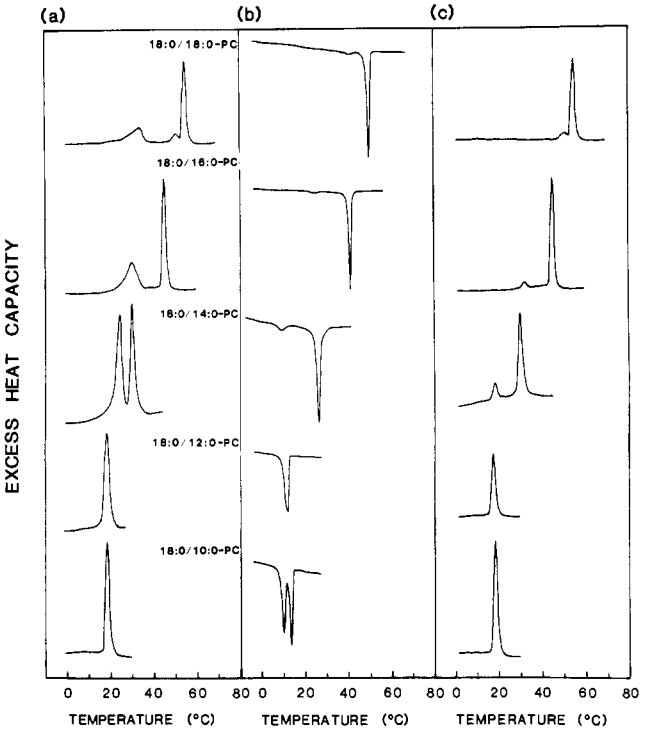


FIGURE 1: DSC scans of 90% hydrated mixed-chain PCs, 18:0/*n*:0-PC ($n$ = 18, 16, 14, 12, or 10), following low-temperature incubation at −4 °C. (a) First heating scans; (b) cooling scans; (c) immediate reheating scans. Heating/cooling rates, 5 °C/min.

several months, at −4 °C prior to transfer to the scanning calorimeter. This time period was sufficient to allow conversion from any metastable states into stable low-temperature phases. In Figure 1a, DSC heating curves are presented for the 18:0/*n*:0-PC series after low-temperature incubation. Panels b and c of Figure 1 show the corresponding cooling and reheating curves obtained immediately after the initial heating.

Following low-temperature incubation for 6 months, 18:0/18:0-PC dispersions show three transitions: a well-defined transition at 33.8 °C ($\Delta H_s$ = 5.2 kcal/mol); a pretransition, $T_p$, at 51.0 °C ($\Delta H_p$ = 1.3 kcal/mol); and a chain melting transition, $T_m$, at 54.7 °C ($\Delta H_m$ = 10.8 kcal/mol). On cooling, as well as on subsequent reheating, only the pretransition and chain melting transition are reversible. The endotherm at ~34 °C is a subtransition ($T_s$) which has been observed previously (Chen et al., 1980; Stümpel et al., 1983; Finegold & Singer, 1984), but at temperatures 2–6 °C lower than the present work. The generation of the subtransition in saturated, identical, and mixed-chain PCs (Ruocco & Shipley, 1982b; Serrallach et al., 1984) was shown to be time and temperature dependent; both transition temperature, $T_s$, and enthalpy, $\Delta H_s$, increase with incubation time, reaching limiting values after prolonged incubation. The higher transition temperature and higher enthalpy for the subtransition of 18:0/18:0-PC in the present work suggest that sufficient time was allowed for low-temperature conversion; however, it is conceivable that even longer incubation could further increase both $T_s$ and $\Delta H_s$.

Like 18:0/18:0-PC, 18:0/16:0-PC also exhibits a subtransition, a pretransition, and a main transition, but the broad subtransition peak ($\Delta H_s$ = 5.5 kcal/mol) occurs close to, and overlaps, the pretransition. For 18:0/14:0-PC, the low-temperature transition occurs about 6 °C higher than the pretransition observed on subsequent cooling and heating, and with an enthalpy greater than that of the main transition. This shift in the main transition temperature toward the subtransition temperature continues for the next member of the series, 18:0/12:0-PC. For 18:0/12:0-PC, a single broad transition is observed at 18.5 °C with a large enthalpy ($\Delta H_s$ = 15.2 kcal/mol). Cooling followed by reheating results in a transition at 17.4 °C, with a considerable reduction in enthalpy, $\Delta H_m$ = 7.6 kcal/mol, and no pretransition is observed. The final member of this series, 18:0/10:0-PC, shows behavior different from that observed with other members of this series. Extensive incubation of 18:0/10:0-PC gives a single transition at 18.4 °C, $\Delta H$ = 9.1 kcal/mol (Figure 1a). On cooling, two transitions are observed at 13.4 and 10.0 °C (combined enthalpy = 9.2 kcal/mol). Subsequent reheating gave a single transition at 18.4 °C ($\Delta H_m$ = 9.1 kcal/mol), and no pretransition is observed. Evidently, for this highly asymmetric PC, a low-temperature phase exhibiting a subtransition is not generated. It should be noted that 18:0/10:0-PC is the only PC of the two series, 18:0/*n*:0-PC and *n*:0/18:0-PC ($n$ = 10 → 18), which did not form a "stable" low-temperature subphase. The reasons for this anomalous behavior are discussed below (see Discussion).

Panels a and b of Figure 3 summarize the transition temperatures and enthalpies, respectively, observed after low-temperature incubation of the 18:0/*n*-0-PC series. The main (chain melting) and pretransition temperatures and their respective enthalpies were determined from the second heating runs (Figure 1c) while the corresponding values for the subtransition were determined from the first heating run after low-temperature annealing (Figure 1a). Note that a subtransition is identified by its appearance on the first heating run following incubation and its disappearance on the second heating run. Some general trends in $T_m$ and $T_p$ are immediately obvious from Figure 3a. $T_m$ decreases as the *sn*-2 chain length is reduced from 18:0 to 12:0 and then increases slightly for 10:0. A similar decrease of $T_p$ with decreasing *sn*-2 chain length is observed for the first three members of this series. 18:0/12:0- and 18:0/10:0-PC do not exhibit a pretransition. $T_s$ also decreases with decreasing *sn*-2 chain length.

The corresponding enthalpy data in Figure 3b show a decrease of $\Delta H_m$ with shortening of the *sn*-2 acyl chain for the first three members of the series, followed by increasing $\Delta H_m$ values for the two shorter chain PCs, 18:0/12:0-PC and 18:0/10:0-PC. There were no significant changes in $\Delta H_p$ for the three members of the series which exhibited a pretransition. However, in contrast, $\Delta H_s$ increases markedly with *sn*-2 chain length reduction.

*n:0/18:0-PC.* Figure 2a–c shows DSC curves for the initial heating, cooling, and reheating scans for the *n*:0/18:0-PC series. Hydrated 16:0/18:0-PC, like 18:0/16:0-PC described above, shows three transitions after low-temperature incubation: a main transition at 49.3 °C ($\Delta H_m$ = 9.2 kcal/mol) and pretransition at 40.6 °C ($\Delta H_p$ = 0.54 kcal/mol), both being reversible, together with a broad subtransition at 37.5 °C ($\Delta H_s$ = 4.4 kcal/mol) not well resolved from the pretransition. Only two transitions are observed for 14:0/18:0-PC: a reversible transition, $T_m$, at 38.2 °C ($\Delta H_m$ = 7.9 kcal/mol) and a transition at 26.4 °C ($\Delta H_s$ = 3.2 kcal/mol) which disappears on cooling and subsequent reheating. The lower transition is clearly a subtransition, and for 14:0/18:0-PC, there is no evidence for the existence of a pretransition on cooling and reheating. For 12:0/18:0-PC after low-temperature incubation, a single broad transition at 24.1 °C with a large enthalpy ($\Delta H_s$ = 13.3 kcal/mol) is observed. The cooling scan shows two transitions at 19.5 °C ($\Delta H$ = 5.2 kcal/mol) and 6.5 °C ($\Delta H$ = 0.3 kcal/mol), while the reheating scan also shows two transitions (11.3 and 23.4 °C) with similar enthalpies to the corresponding exotherms. The lower transition is a pretran-

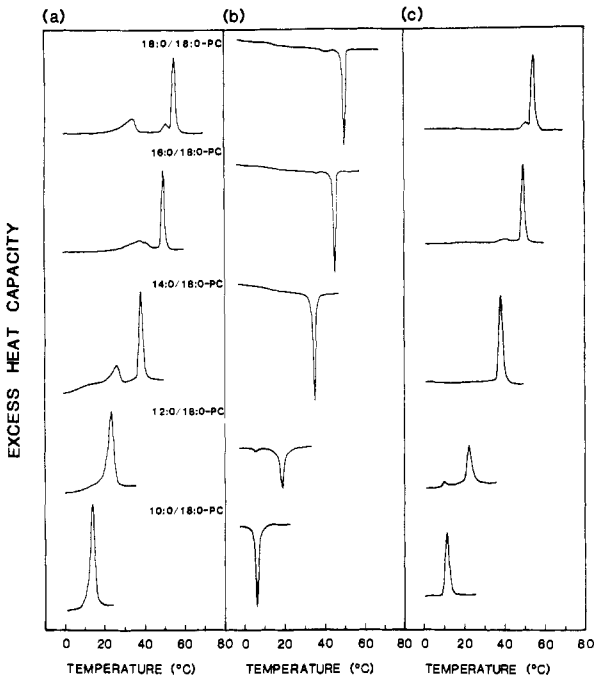


FIGURE 2: DSC scans of 90% hydrated mixed-chain PCs, *n*:0/18:0-PC (*n* = 18, 16, 14, 12, or 10), following low-temperature incubation at −4 °C. (a) First heating scans; (b) cooling scans; (c) immediate reheating scans. Heating/cooling rates, 5 °C/min.

sition, judging from its reversibility and low enthalpy, while after incubation a "subtransition" occurs at 24.1 °C, with a high enthalpy ($\Delta H_s$ = 13.3 kcal/mol). The presence of a pretransition for 12:0/18:0-PC is unexpected, since the general trend is the disappearance of the pretransition with decreasing chain length for both PC series (see Figure 3a) and 14:0/18:0-PC does not show a pretransition. The formation of a low-temperature phase with a transition temperature greater than that of the main transition is also unusual for PCs, although this behavior was observed with phosphatidylethanolamines (Wilkinson & Nagle, 1984; Seddon et al., 1983). The highly asymmetric 10:0/18:0-PC shows a transition at 14.1 °C ($\Delta H_s$ = 11.8 kcal/mol) after incubation; the cooling scan gave a transition at 7.3 °C ($\Delta H$ = 6.5 kcal/mol), while a single sharp transition, also with a much reduced enthalpy, $T_m$ = 12.4 °C ($\Delta H_m$ = 6.6 kcal/mol), is observed in the heating scan following cooling.

The transition temperatures and enthalpies for the *n*:0/18:0-PC series are plotted as a function of *sn*-1 chain length in Figure 3a,b. The $T_m$ determined from Figure 2c decreases with *sn*-1 chain length reduction; a similar reduction in $T_p$ with chain length is observed for 16:0/18:0-PC and 12:0/18:0-PC. A reduction in transition enthalpy ($\Delta H_m$) with *sn*-1 chain length is also observed for the first four members of the series, 18:0/18:0-PC to 12:0/18:0-PC, while 10:0/18:0-PC has a slightly higher enthalpy than 12:0/18:0-PC. The enthalpy of the pretransition is essentially independent of *sn*-1 chain length. There is a marked discontinuity between 14:0/18:0-PC and 12:0/18:0-PC in the dependence of $\Delta H_s$ with chain length (Figure 3b).

### *X-ray Diffraction of Hydrated (~50 wt % Water) Saturated Mixed-Chain PCs, 18:0/n:0-PC and n:0/18:0-PC (n = 18, 16, 14, 12, or 10)*

Following low-temperature incubation, DSC demonstrated the formation of at least two, and at most four, phases for mixed-chain PCs, depending on the length of the variable chain. In this section, we have characterized by X-ray diffraction the structures that gave rise to the various phase changes shown in Figures 1 and 2.

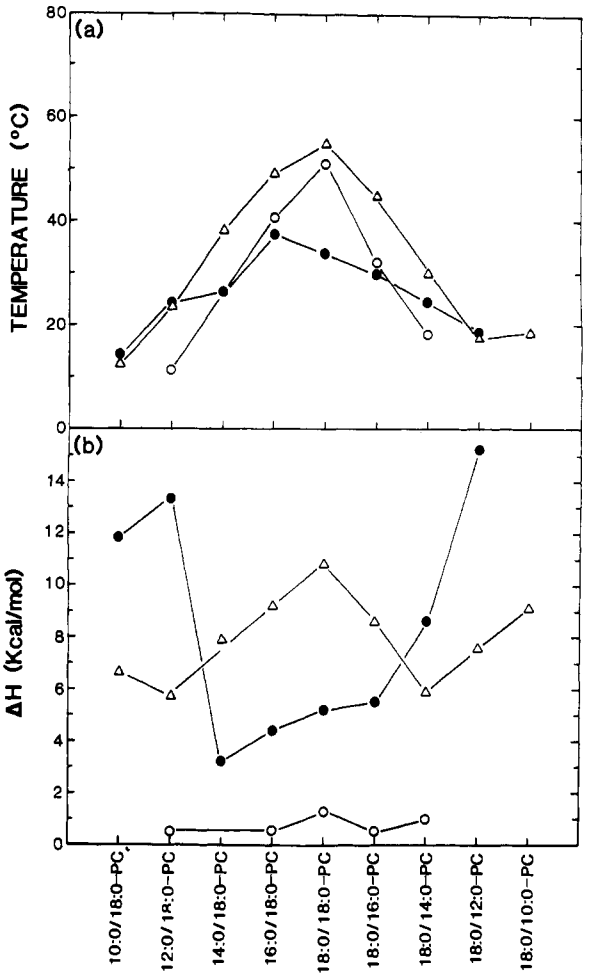


FIGURE 3: Variation of transition temperatures (a) and transition enthalpies (b) as a function of acyl chain length reduction in the *sn*-1 and *sn*-2 positions of the glycerol backbone for the two series of mixed-chain PCs, 18:0/*n*:0-PC and *n*:0/18:0-PC (*n* = 18, 16, 14, 12, or 10). (Δ) Main transition temperature, $T_m$, and enthalpy, $\Delta H_m$; (○) pretransition temperature, $T_p$, and enthalpy, $\Delta H_p$; (●) subtransition temperature, $T_s$, and enthalpy, $\Delta H_s$. (Calorimetric parameters derived from initial and reheating scans of Figures 1 and 2.)

*18:0/n:0-PC.* The four phases observed for 18:0/18:0-PC by DSC (Figure 1a) are typical of a PC with identical saturated chains in the *sn*-1 and *sn*-2 positions. For example, 16:0/16:0-PC also showed three endothermic transitions after low-temperature incubation (Ruocco & Shipley, 1982b). In Figure 4a–d, X-ray diffraction patterns at −4, 41, 50, and 65 °C are presented for fully hydrated 18:0/18:0-PC. The X-ray sample was incubated at −4 °C for ~6 months prior to the recording of the diffraction pattern at −4 °C.

The diffraction patterns at the four temperatures are indicative of lamellar geometries (see low-angle region) but differ from each other in the wide-angle region, indicating different chain packing modes. At −4 °C, the low-angle region shows eight diffraction spacings in the ratio $1:{}^1/_2:{}^1/_3:{}^1/_4$ etc. corresponding to a bilayer periodicity, 18:0/18:0-PC bilayer plus intercalated water, $d$ = 65.5 Å (Figure 4a). The wide-angle region shows three strong reflections at 4.44, 4.19, and 3.90 Å (arrowed), together with an additional reflection at 6.80 Å. This is indicative of a crystalline bilayer phase, $L_c$, with specific lateral intra- and intermolecular interactions. This type of crystalline bilayer phase was also observed for 16:0/16:0-PC (Füldner, 1981; Ruocco & Shipley, 1982a,b) and other positional isomers (Stümpel et al., 1983; Serrallach et al., 1984),

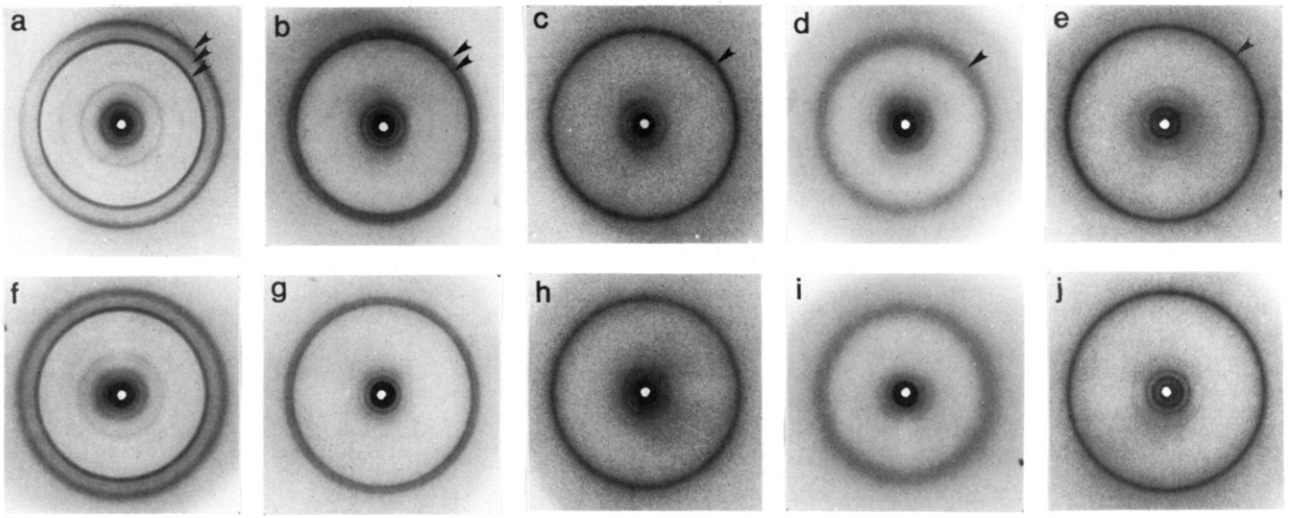


FIGURE 4: X-ray diffraction patterns of the different phases obtained for identical and mixed-chain PCs at 50% hydration. (a–d) $L_c$, $L_{\beta}'$, $P_{\beta}'$, and $L_{\alpha}$ phases of 18:0/18:0-PC at −4, 41, 50, and 65 °C; (e) $L_{\beta}$* phase of 18:0/10:0-PC at −4 °C; (f) $L_c$ phase of 14:0/18:0-PC at −4 °C; (g) $L_{\beta}'$ phase of 18:0/14:0-PC at 7 °C following cooling; (h) $P_{\beta}'$ phase of 18:0/16:0-PC at 38 °C; (i) $L_{\alpha}$ phase of 16:0/18:0-PC at 55 °C; (j) $L_{\beta}$* phase of 18:0/12:0-PC at 8 °C.

where the acyl chains have crystallized laterally into an ordered chain packing mode described by one of the specific, complex subcells (Abrahamsson et al., 1964, 1978). 18:0/18:0-PC at 41 °C shows five lamellar low-angle reflections, characteristic of a bilayer structure, $d$ = 68.1 Å (Figure 4b). The wide-angle region shows two reflections: a sharp band at 4.26 Å and a more diffuse and almost overlapping band at 4.03 Å (arrowed). This wide-angle pattern is characteristic of an $L_{\beta}'$ bilayer gel phase with tilted hydrocarbon chains (Tardieu et al., 1973; Janiak et al., 1979). The diffraction pattern of 18:0/18:0-PC at 50 °C, between the pretransition and main transition temperatures, shows bilayer geometry in the low-angle region ($d$ = 70.3 Å), with a single wide-angle reflection at 4.18 Å (arrowed) indicative of hexagonal chain packing (Figure 4c). A similar diffraction pattern is observed for 16:0/16:0-PC and 14:0/14:0-PC between the pretransition and main transition temperature (Janiak et al., 1976, 1979) and is representative of a two-dimensional rippled bilayer gel phase. This rippled bilayer phase is characterized at lower water content by additional weak reflections in the low-angle region due to the ripple structure. At 64 °C, above the chain melting transition, four lamellar reflections, $d$ = 66.9 Å, are observed while the wide-angle region shows a broad diffuse band at 4.5 Å (arrowed; see Figure 4d). This diffraction pattern is characteristic of the liquid-crystalline $L_{\alpha}$ bilayer phase with melted hydrocarbon chains. On cooling, both the main transition and pretransition are reversible (see Figure 1), and the X-ray diffraction pattern below $T_m$ is identical with that of the rippled gel phase (cf. Figure 4c). This gel phase transforms to the tilted gel phase, $L_{\beta}'$ (cf. Figure 4b), on further cooling to 25 °C and eventually forms the crystalline $L_c$ phase on low-temperature incubation.

The phases giving rise to the endothermic and exothermic transitions shown in Figures 1 and 2 for the series of mixed-chain PCs were also characterized by X-ray diffraction. Diffraction patterns representative of other $L_c$, $L_{\beta}'$, $P_{\beta}'$, and $L_{\alpha}$ phases, selected from different mixed-chain PCs, are shown in Figure 4f–i. Also shown in Figure 4e,j are the X-ray diffraction patterns of a novel interdigitated, three chains per head group bilayer gel phase, $L_{\beta}$* (McIntosh et al., 1984; Hui et al., 1984), recorded for 18:0/10:0-PC and 18:0/12:0-PC. In Table I, a summary of the diffraction spacings for the wide-angle region and the bilayer repeat distance, $d$, at appropriate temperatures is presented for the two series. The different phases, identified from the diffraction patterns, are also presented in Table I.

On low-temperature incubation, the 18:0/*n*:0-PCs form crystalline phases as the *sn*-2 chain length decreases from 18:0 to 12:0. These phases, although similar, are not exactly isomorphous as is evident from the different wide-angle spacings observed for each PC (see Table I). The most asymmetric member of the series, 18:0/10:0-PC, shows a single wide-angle reflection at 4.1 Å (arrowed), which is incubation time independent (see Figure 4e). This single reflection, together with a short bilayer repeat distance of 53.6 Å, is characteristic of the $L_{\beta}$* phase reported recently for 18:0/10:0-PC (McIntosh et al., 1984; Hui et al., 1984). Both DSC and X-ray measurements indicate that the $L_{\beta}$* phase of 18:0/10:0-PC does not transform into a crystalline phase at low temperature. Above the chain melting transition temperature, liquid-crystalline $L_{\alpha}$ phases are observed for all the 18:0/*n*:0-PCs (see Figure 4d,i). Below $T_m$, a number of different gel phases, which are either tilted, $L_{\beta}'$ (Figure 4b,g), rippled, $P_{\beta}'$ (Figure 4c,h), or triple chain, $L_{\beta}$* (Figure 4e,j), are present, and the structures adopted by these different gel phases are chain length dependent (see Table I). In most cases, the gel phases convert into stable crystalline bilayer phases on incubation at low temperature.

Figure 5a shows schematically the structural changes exhibited by the 18:0/*n*:0-PC series at 50% hydration. As noted above, 18:0/18:0-PC shows a subtransition which is distinctly separated from the pretransition by 20 °C. Four distinct phases are observed on heating. Note that on cooling the transformation to a crystalline $L_c$ phase occurs via a tilted gel phase, $L_{\beta}'$. As the hydrocarbon chain length in the *sn*-2 position of the glycerol backbone is reduced by two methylene groups (18:0/16:0-PC), the subtransition and pretransition overlap (see Figure 1), and only three phases are observed by X-ray diffraction on heating (for the $P_{\beta}'$ phase, see Figure 4h); note the absence of an $L_{\beta}'$ gel phase on heating and its appearance on cooling below the pretransition. The $L_{\beta}'$ phase eventually transforms to the low-temperature crystalline phase, a behavior similar to that observed for 18:0/18:0-PC. The structural transformations of 18:0/14:0-PC are identical with those of 18:0/16:0-PC. As the hydrocarbon chains become more asymmetric, for 18:0/12:0-PC the number of structural transformations on heating and cooling is reduced. The crystalline $L_c$ phase changes to the liquid-crystalline $L_{\alpha}$ phase

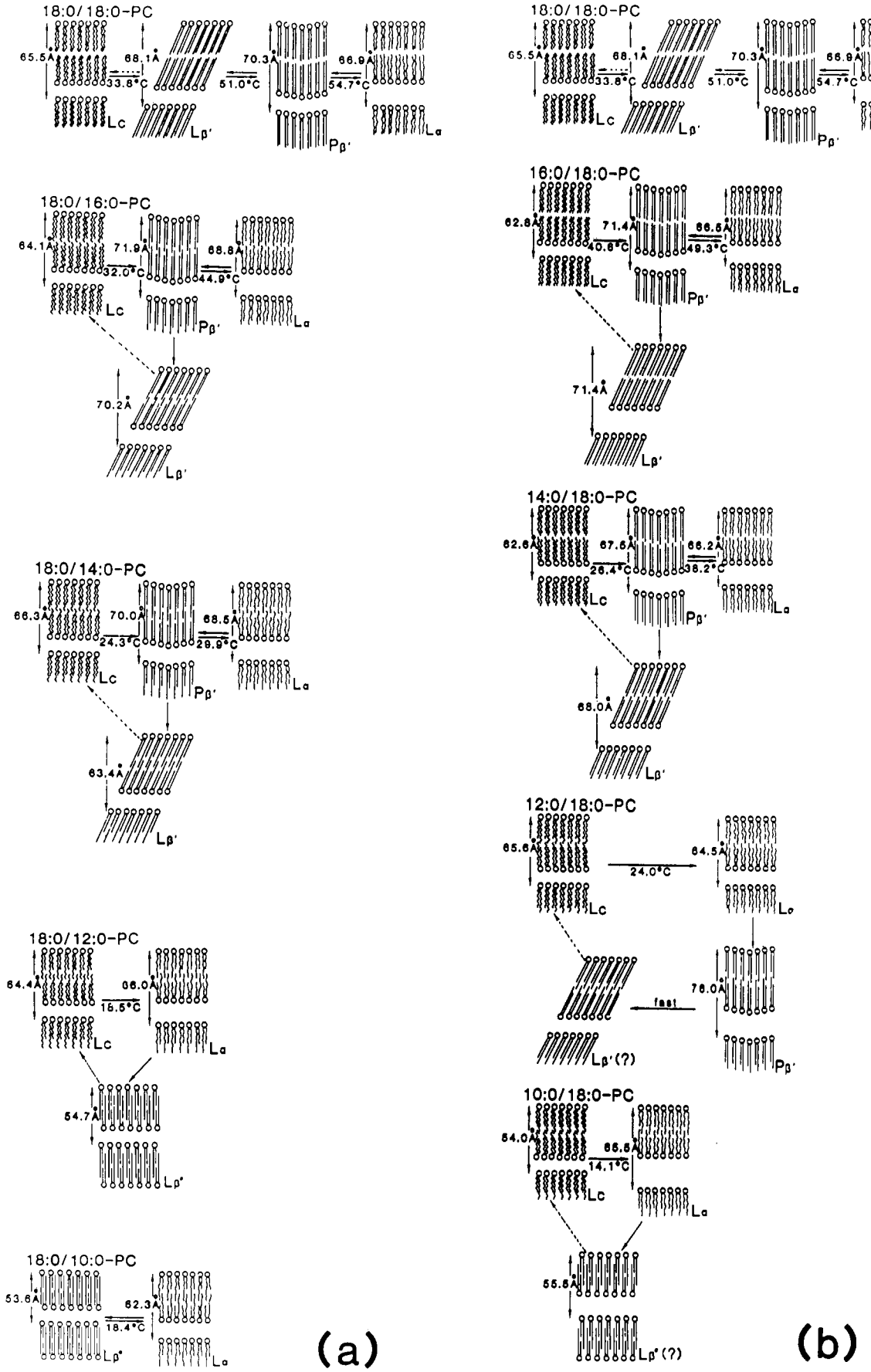


FIGURE 5: Schematic representation of the structural changes exhibited by 50% hydrated mixed-chain PCs with increasing and decreasing temperatures. (a) 18:0/*n*:0-PC and (b) *n*:0/18:0-PC (*n* = 18, 16, 14, 12, or 10). (〰) represents crystalline chain packing; (—) represents rotationally disordered chain packing; and (~), represents melted chains. Dashed arrows represent slow conversions to $L_c$ phases.

Table I: Wide-Angle Diffraction Spacings and Bilayer Periodicity of 50% Hydrated 18:0/*n*:0-PC and *n*:0/18:0-PC (*n* = 18, 16, 14, 12, or 10) at Several Temperatures following Incubation at −4 °C

| PC | temp (°C) | phase | wide-angle reflections (Å) | bilayer periodicity (Å) |
|---|---|---|---|---|
| 18:0/18:0-PC | −4 | $L_c$ | 4.44, 4.19, 3.90 | 65.5 |
| | 41 | $L_{\beta'}$ | 4.26, 4.03 | 68.1 |
| | 50 | $P_{\beta'}$ | 4.18 | 70.3 |
| | 65 | $L_\alpha$ | 4.55 | 66.9 |
| | 45[a] | $P_{\beta'}$ | 4.18 | 70.5 |
| | 25[a] | $L_{\beta'}$ | 4.26, 4.03 | 68.0 |
| 18:0/16:0-PC | −4 | $L_c$ | 5.24, 4.57, 3.94 | 64.1 |
| | 30 | $P_{\beta'}$ | 4.29 | 71.3 |
| | 38 | $P_{\beta'}$ | 4.29 | 71.9 |
| | 52 | $L_\alpha$ | 4.57 | 68.8 |
| | 35[a] | $P_{\beta'}$ | 4.28 | 71.6 |
| | 16[a] | $L_{\beta'}$ | 4.35, 4.23 | 70.2 |
| 18:0/14:0-PC | −4 | $L_c$ | 4.54, 4.29, 4.01, 3.76 | 66.3 |
| | 24 | $P_{\beta'}$ | 4.21 | 70.0 |
| | 35 | $L_\alpha$ | 4.50 | 68.5 |
| | 20[a] | $P_{\beta'}$ | 4.19 | 70.2 |
| | 7[a] | $L_{\beta'}$ | 4.25, 4.06 | 63.4 |
| 18:0/12:0-PC | −4 | $L_c$ | 4.53, 4.24, 3.76 | 64.4 |
| | 25 | $L_\alpha$ | 4.50 | 66.0 |
| | 8[a] | $L_\beta$* | 4.11 | 54.7 |
| 18:0/10:0-PC | −4 | $L_\beta$* | 4.11 | 53.6 |
| | 25 | $L_\alpha$ | 4.48 | 62.3 |
| | 5[a] | $L_\beta$* | 4.11 | 53.9 |
| 18:0/18:0-PC | −4 | $L_c$ | 4.44, 4.19, 3.90 | 65.5 |
| | 41 | $L_{\beta'}$ | 4.26, 4.03 | 68.1 |
| | 50 | $P_{\beta'}$ | 4.18 | 70.3 |
| | 65 | $L_\alpha$ | 4.55 | 66.9 |
| | 45[a] | $P_{\beta'}$ | 4.18 | 70.5 |
| | 25[a] | $L_{\beta'}$ | 4.26, 4.03 | 68.0 |
| 16:0/18:0-PC | −4 | $L_c$ | 5.09, 4.52, 3.97, 3.73 | 62.8 |
| | 36 | $L_c$ | 4.51, 4.23, 3.79 | 63.5 |
| | 42 | $P_{\beta'}$ | 4.26 | 71.4 |
| | 55 | $L_\alpha$ | 4.54 | 66.5 |
| | 37[a] | $P_{\beta'}$ | 4.22 | 71.9 |
| | 22[a] | $L_{\beta'}$ | 4.41, 4.27 | 71.4 |
| 14:0/18:0-PC | −4 | $L_c$ | 4.50, 4.20, 3.86 | 62.6 |
| | 30 | $P_{\beta'}$ | 4.21 | 67.5 |
| | 45 | $L_\alpha$ | 4.51 | 66.2 |
| | 28[a] | $P_{\beta'}$ | 4.21 | 67.5 |
| | 8[a] | $L_{\beta'}$ | 4.48, 4.20 | 68.0 |
| 12:0/18:0-PC | −4 | $L_c$ | 4.56, 4.27, 4.0, 3.8 | 65.8 |
| | 13 | $L_c$ | 4.56, 4.27, 4.0, 3.8 | 65.8 |
| | 32 | $L_\alpha$ | 4.51 | 64.5 |
| | 13[a] | $P_{\beta'}$ | 4.28 | 76.0 |
| 10:0/18:0-PC | −4 | $L_c$ | 4.56, 4.15, 3.82 | 54.0 |
| | 22 | $L_\alpha$ | 4.51 | 65.5 |
| | 5[a] | $L_\beta$* (?) | 4.23 | 55.8 |

[a] Following cooling from the $L_\alpha$ phase.

at 18.5 °C without the formation of intermediate gel phases. The diffraction pattern obtained on cooling to 8 °C shows a single wide-angle reflection at 4.1 Å together with lamellar reflections in the low-angle region, $d$ = 54.7 Å (see Figure 4j). This diffraction pattern is identical with that observed for the highly asymmetric 18:0/10:0-PC (see Figure 4e). Below 13.6 °C, 18:0/12:0-PC exists in an interdigitated $L_\beta$* phase (see Figure 4j) which is transformed to the crystalline $L_c$ bilayer phase at low temperatures. Finally, for the most asymmetric member of the series, 18:0/10:0-PC, no crystalline phases are observed even after months of low-temperature incubation. Instead, the triple-chain interdigitated structure, $L_\beta$* (Figure 4e), is the most stable structure below the main transition, and only the reversible phase change, $L_\beta$* ↔ $L_\alpha$, is observed.

*n:0/18:0-PC.* The X-ray diffraction data for the *n*:0/18:0-PC series are summarized in Table I, and the structural changes are shown schematically in Figure 5b. All members of the *n*:0/18:0-PC series are transformed into crystalline phases at low temperature. Individually, 16:0/18:0-PC showed similar phase behavior to its positional isomer 18:0/16:0-PC; a subtransition is observed (see Figure 2a) which is superimposed on the pretransition, and only three different phases, $L_c$, $P_{\beta'}$, and $L_\alpha$ (see Figure 4i), are observed on heating (Figure 5b). On cooling, the $L_c$ phase is formed from a metastable, tilted gel phase. There is no observable pretransition for 14:0/18:0-PC (see Figure 2c), and the X-ray diffraction data showed a structural transformation at 26.4 °C from an $L_c$ phase (see Figure 4f) to an untilted gel phase. We have not determined whether this is a rippled gel phase, but the intensity distribution of the lamellar reflections and the single 4.21-Å wide-angle reflection are similar to the rippled gel phases formed by other PCs. The rippled gel → $L_\alpha$ transformation is reversible, and on cooling to lower temperatures, a tilted-chain bilayer gel phase is observed at 15 °C. Apparently, an untilted gel phase is first converted to a tilted gel phase before transformation to the crystalline phase, although no calorimetric evidence for the gel–gel transition is observed (see Figure 2b). 12:0/18:0-PC, like its positional isomer 18:0/12:0-PC, is transformed to the $L_\alpha$ phase directly from a crystalline $L_c$ phase. However, on cooling and reheating (Figure 2b,c), a pretransition is observed, and the X-ray diffraction pattern at 13.0 °C is probably that of a rippled gel phase ($d$ = 76.0 Å). The transformation to the crystalline phase is relatively fast below the pretransition temperature of 6.5 °C, and hence, the gel phase structure, from which the $L_c$ phase is formed, has not been determined. The crystalline phase of the most asymmetric member of the series, 10:0/18:0-PC, has an unusually short bilayer repeat distance of 54.0 Å, compared with 65.8 Å for the $L_c$ phase of 12:0/18:0-PC. This $L_c$ phase is converted to the $L_\alpha$ phase above 14.1 °C; on cooling below 7.3 °C, a gel phase with untilted hydrocarbon chains and a short repeat distance of 56.0 Å, similar to that observed in Figure 4e for the triple chain, interdigitated three chains per head-group gel phase, $L_\beta$*, is observed. This phase is metastable and converts to the $L_c$ phase at low temperatures.

## Discussion

Calorimetric studies of two series of saturated mixed-chain PCs, 18:0/*n*:0-PC and *n*:0/18:0-PC, show that the temperature and enthalpy of the main transition are dependent on the length of the fatty acyl chains and their distribution on the glycerol backbone. The transition temperature ($T_m$) progressively decreases as the chain length decreases from 18:0 to 10:0 for the series *n*:0/18:0-PC (Figure 3a). A similar decrease in $T_m$ with chain length is also observed for the first four members of the series, 18:0/*n*:0-PC (*n* = 18, 16, 14, or 12), but the $T_m$ for 18:0/10:0-PC is 1 °C higher than that for 18:0/12:0-PC (Figure 3a). For both series, the transition enthalpies ($\Delta H_m$) also decrease with chain length reduction for the longer acyl chain lipids; however, the shorter chain lipids (18:0/12:0-PC, 18:0/10:0-PC, and 10:0/18:0-PC) have a higher transition enthalpy than the preceding members of their respective series (Figure 3b).

A comparison of the two series of PCs, 18:0/*n*:0-PC and *n*:0/18:0-PC, showed that the PC with the longer fatty acyl chain in the *sn*-2 position of the glycerol backbone has the higher $T_m$ (see Figure 3a); the exception is for *n* = 10, where 18:0/10:0-PC has a $T_m$ higher by 6 °C than its positional isomer, 10:0/18:0-PC. The length and distribution of the fatty acyl chains and their effects on the $T_m$ of mixed-chain PCs have been noted previously (Keough & Davis, 1979; Mason et al., 1981b; Huang et al., 1983; Chen & Sturtevant, 1981; Stümpel et al., 1983) and are related to optimal packing of the hydrocarbon chains for maximum van der Waals contact (see below).

The chain length distribution also affects the pretransition temperature significantly, but not the transition enthalpy (see Figure 3a,b). Pretransitions are observed for 18:0/18:0-PC, 18:0/16:0-PC, and 18:0/14:0-PC, but not for the lower members of this series, with $T_p$ progressively decreasing with chain length. Pretransitions were also observed for 16:0/18:0-PC and 12:0/18:0-PC but, surprisingly, not for the intermediate member of the series, 14:0/18:0-PC. A comparison of $T_p$ for the only two positional isomers which gave pretransitions, 18:0/16:0-PC and 16:0/18:0-PC, suggests that the PC with the longer fatty acid in the *sn*-2 position of the glycerol backbone has a higher $T_p$.

Crystalline bilayer phases are formed at low temperatures for both series, 18:0/*n*:0-PC and *n*:0/18:0-PC, except 18:0/10:0-PC. Previous studies of symmetric and asymmetric PCs have shown the formation of crystalline, dehydrated phases at low temperatures (Chen et al., 1980; Füldner, 1981; Ruocco & Shipley, 1982a,b; Stümpel et al., 1983; Serrallach et al., 1984; Finegold & Singer, 1986). Crystalline phases have also been observed with other saturated chain phospholipids including phosphatidylethanolamine (Chang & Epand, 1983; Wilkinson & Nagle, 1984; Seddon et al., 1983) and phosphatidylglycerol (Wilkinson & McIntosh, 1986; Blaurock & McIntosh, 1986). We now show that the subtransition enthalpy ($\Delta H_s$) and temperature ($T_s$) are dependent on the fatty acyl chain length and the distribution of fatty acids on the glycerol backbone (see Figure 3). As the length of the hydrocarbon chain is reduced on the *sn*-2 position, at least, the subtransition enthalpies increase (see Figure 3b). The temperature at which the subtransition occurs is also chain length dependent. In general, $T_s$ decreases as the chain length in either the *sn*-1 or the *sn*-2 position is reduced (note that 16:0/18:0-PC is an exception; see Figure 3a). Note also that $T_s$ is gradually shifted toward $T_m$ as the chain length is decreased and occurs slightly above the main transition temperature of the more asymmetric PCs, 18:0/12:0-PC, 12:0/18:0-PC, and 10:0/18:0-PC. Similar behavior has been observed for symmetric PCs with $T_s$ being higher than $T_m$ for 12:0/12:0-PC (Finegold & Singer, 1986). The crystalline phases for these PCs are therefore more stable than all their gel phases. While the kinetics of formation of the crystalline phases were not examined in detail, the PCs with shorter hydrocarbon chains on either the *sn*-1 or the *sn*-2 positions are more rapidly converted to the $L_c$ phases; for example, for 18:0/12:0-PC, 12:0/18:0-PC, and 10:0/18:0-PC, the conversion occurred within a few hours at −4 °C compared to several days for the longer chain PCs.

Crystalline $L_c$ phases, stabilized by specific chain packing modes, are observed for all the mixed-chain PCs, with the exception of 18:0/10:0-PC. While the wide-angle reflections are not identical for the different PCs, the presence of two reflections at 4.4–4.5 and 3.8–3.9 Å is a common feature of all the $L_c$ phases (see Table I). These two reflections were also observed for the $L_c$ phases of 16:0/16:0-PC (Füldner, 1981; Ruocco & Shipley, 1982a,b), 14:0/16:0-PC, and 16:0/14:0-PC (Serrallach et al., 1984), suggesting a similar chain packing mode for all PCs in their annealed phases. The $L_\alpha \rightarrow L_c$ conversion occurs through a number of phase changes which are chain length dependent. 18:0/18:0-PC is transformed on heating from the $L_c$ phase to the "distorted" hexagonal or orthorhombic chain packing mode of the $L_{\beta'}$ phase; further heating produces the hexagonal chain packing mode of the rippled $P_{\beta'}$ phase and finally chain melting to the $L_\alpha$ phase. The positional isomers 18:0/16:0-PC and 16:0/18:0-PC show broad subtransitions which superimpose on the pretransition (Figures 1 and 2); presumably, the $L_c$ phases of these lipids are transformed to $L_{\beta'}$ phases (similar to that observed for 18:0/18:0-PC, although not resolved in the X-ray diffraction experiments) and are then rapidly transformed into a rippled gel phase followed by the $L_\alpha$ phase (see Figure 5a,b). As the chain length is further reduced by two methylene groups (18:0/14:0-PC and 14:0/18:0-PC), the $L_c$ phase directly transforms to the rippled gel phase followed by the $L_\alpha$ phase on heating. The direct conversion of the $L_c$ phase to the $P_{\beta'}$ phase without formation of the intermediate $L_{\beta'}$ gel phase has been previously observed for 14:0/18:0-PC by solid-state NMR (Lewis et al., 1984). For the shorter chain PCs, 18:0/12:0-PC, 12:0/18:0-PC, and 10:0/18:0-PC, only the single transformation $L_c \rightarrow L_\alpha$ is observed.

On cooling, the $L_\alpha \rightarrow P_{\beta'}$ transition is readily reversible for the PCs which show a rippled gel phase. However, the conversion to the $L_c$ phase does not occur from the rippled gel phase. The X-ray diffraction data show that the $L_c$ phases of 18:0/18:0-PC, 18:0/16:0-PC, 18:0/14:0-PC, 16:0/18:0-PC, and 14:0/18:0-PC are formed from tilted bilayer $L_{\beta'}$ gel phases (see Figure 5a,b). The formation of crystalline phases from tilted gel phases at low temperature has been previously reported for 16:0/16:0-PC (Ruocco et al., 1982a,b) and 16:0/14:0-PC and 14:0/16:0-PC (Serrallach et al., 1984). The precise structure of these tilted gel phases is dependent on chain length and chain distribution on the glycerol backbone. Hydrocarbon chain tilt occurs in PCs, in part at least because the choline head group, lying parallel to the bilayer plane (Franks, 1976; Büldt et al., 1978; McIntosh, 1980), has a larger surface area than the two chains.

The chain length dependence of the tilted gel phase is related to the conformational inequivalence of the two acyl chains (Hitchcock et al., 1974; Elder et al., 1977; Pearson & Pascher, 1979); the initial segment of the *sn*-2 chain is perpendicular to the *sn*-1 chain, and neutron diffraction (Büldt et al., 1978; Zaccai et al., 1979) has established that the *sn*-1 chain is longer than the *sn*-2 chain by approximately three methylene groups in the center of the bilayer for identical chain PCs. The difference in chain length becomes more pronounced as the length of the *sn*-2 acyl chain is reduced; for 18:0/16:0-PC and 18:0/14:0-PC, these differences are five and seven methylene groups, respectively. To maximize van der Waals contacts in the gel phase, there must be progressive interdigitation of the acyl chains across the center of the bilayer for the 18:0/*n*:0-PC series ($n$ = 18, 16 or 14), as indicated from other studies of mixed-chain PCs (Chen & Sturtevant, 1981; Mason et al., 1981b; Huang et al., 1983; Hui et al., 1984). This point is illustrated in the molecular models of bilayers for the 18:0/*n*:0-PC series, shown in Figure 6a–c. In the absence of interdigitation, an energetically unfavorable chain packing situation would occur with voids created toward the terminal methyl groups.

For 16:0/18:0-PC and 14:0/18:0-PC, the chain length difference between the *sn*-1 and *sn*-2 chains at the center of the bilayer is plus one methylene and minus one methylene group, respectively. This would allow for minimum interdigitation with better packing in the bilayer for these PCs in their gel phase. For other members of the two series, interdigitation allows for better molecular packing, but it has the disadvantage of placing the terminal methyl group adjacent to methylene groups in the bilayer (see Figure 6a–c). This would disrupt chain packing in this region of the bilayer, since the volume of a methyl group is approximately twice that of a methylene group (Tardieu et al., 1973). Huang et al. (1983) have shown by Raman spectroscopy that 18:0/14:0-PC, for example, has

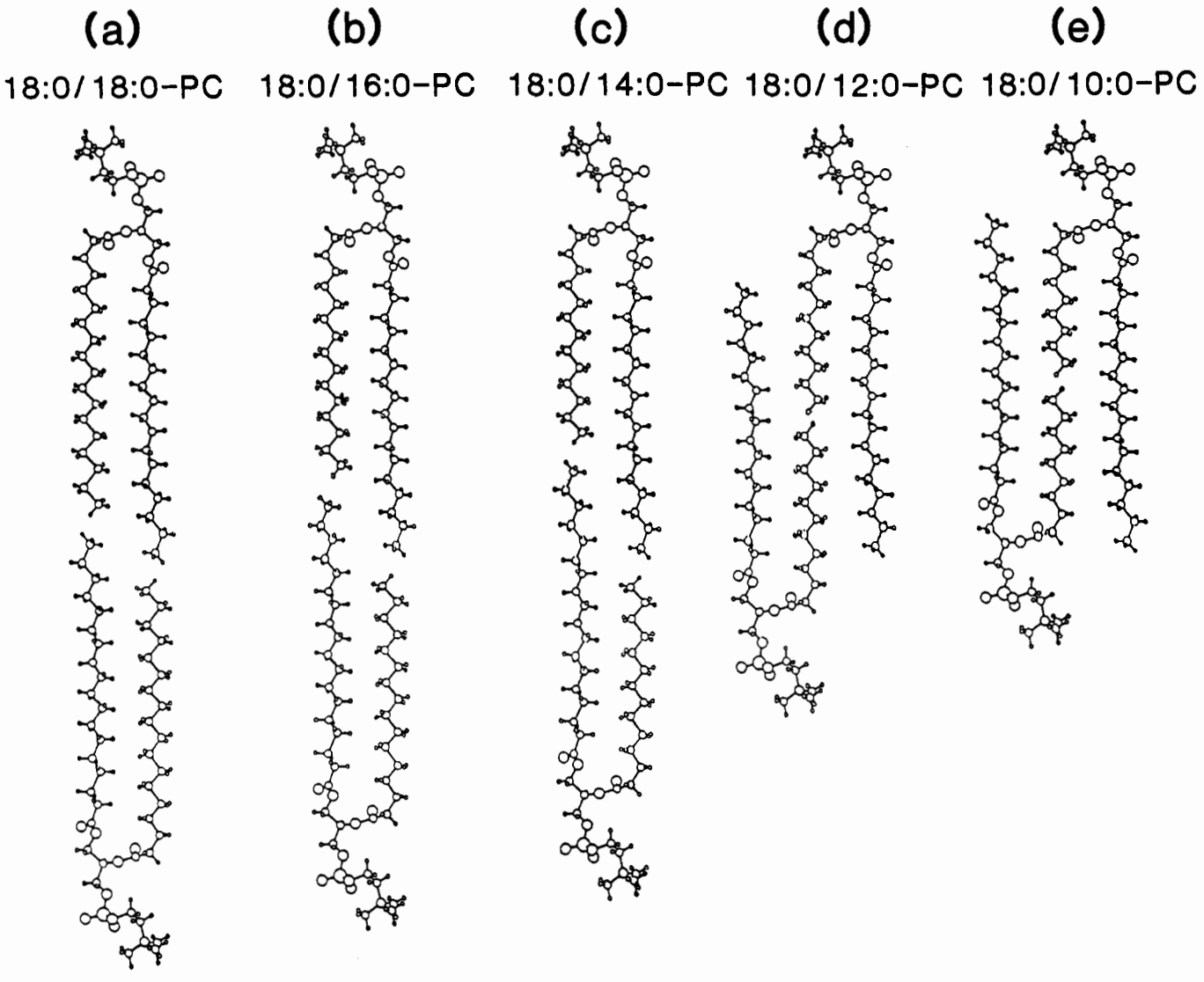


FIGURE 6: Molecular models [based on the structure of 14:0/14:0-PC; see Pearson and Pascher (1979)] of gel phase bilayers for the 18:0/*n*:0-PC (*n* = 18, 16, 14, 12, and 10) series, showing progressive acyl chain interdigitation with chain length reduction and the eventual formation of the triple-chain structure.

a greater gauche bond population near the terminal methyl groups, implying greater disorder in this region of the bilayer. This concept was suggested originally by Keough and Davis (1979) for mixed-chain PCs on the basis of calorimetric data. The difference in transition temperature between the positional isomers (e.g., 18:0/16:0-PC and 16:0/18:0-PC, and 18:0/14:0-PC and 14:0/18:0-PC) could be manifestations of the different degrees of interdigitation. The PCs with the greater requirement for interdigitation have the lower transition temperature and enthalpy, in agreement with the calorimetric data for these positional isomers (see Figure 3a,b). The tilted gel phase, $L_{\beta}'$, is the metastable state for the longer chain PCs (*n* = 18, 16, or 14). It is conceivable that the $L_c$ phase of 12:0/18:0-PC is also formed from a tilted but partially interdigitated gel phase, since the *sn*-1 chain extends into the bilayer about three methylene groups less than the *sn*-2 chain.

The three chains per head-group gel phase, $L_{\beta}$*, is the metastable state for 18:0/12:0-PC, while it is the stable phase for the most asymmetric of the mixed-chain PCs, 18:0/10:0-PC. The $L_{\beta}$* structure of 18:0/10:0-PC is possible because the two apposing decanoyl chains at the *sn*-2 position have an effective length of 17 C–C bonds; this length, together with the 2-Å separation of the terminal methyl groups, is exactly matched by the length of one stearoyl chain in an all-trans conformation and allows for maximum chain–chain interaction [see Figure 6e and McIntosh et al. (1984) and Hui et al. (1984)]. The larger enthalpy and entropy change observed for this asymmetric PC (Figure 3b) on chain melting is presumably due to the strong chain–chain interactions of the $L_{\beta}$* phase. Although the $L_{\beta}$* phase is the most stable gel phase of 18:0/10:0-PC, we note that it exhibits two exothermic transitions on cooling (see Figure 1b), suggesting the formation of some intermediate between the $L_{\alpha}$ and $L_{\beta}$* phases. The stability of the $L_{\beta}$* phase was also noted for the highly asymmetric ether-linked 1-eicosyl-2-dodecyl-*rac*-glycero-3-phosphocholine (Mattai et al., 1987) with a similar asymmetry of eight methylene groups between the *sn*-1 and *sn*-2 chains.

In contrast, the $L_{\beta}$* phase of 18:0/12:0-PC is metastable and is transformed to an ordered phase at low temperature. The reason for this metastability is the increased length of the *sn*-2 chains (Figure 6d); 2 dodecanoyl chains spanning the bilayer in the triple-chain structure have an effective thickness of 21 C–C bonds plus 2 Å between terminal methyl groups. This is about four C–C bonds longer than the length of the stearoyl chain. The resulting $L_{\beta}$* structure does not permit optimum van der Waals interaction, since methylene groups of the *sn*-2 chains toward the head-group region do not have adjacent *sn*-1 methylene groups for interaction (cf. Figure 6d,e). Low-temperature incubation transforms this metastable gel phase to a stable, two chains per head-group $L_c$ phase.

Finally, the diffraction pattern for 10:0/18:0-PC below the $L_\alpha$ phase is similar to those of 18:0/10:0-PC and 18:0/12:0-PC in their $L_\beta$* phases. It is not apparent why 10:0/18:0-PC should form a triple-chain structure, since its formation would considerably reduce chain–chain interaction and create voids toward the head-group region of the bilayer. Recent ESR spin-label studies by Boggs and Mason (1986) also suggest an interdigitated gel phase structure for 10:0/18:0-PC, as well as for 18:0/10:0-PC and 18:0/12:0-PC.

Thus, the gel phases, $L_\beta'$ and $L_\beta$*, interdigitate, albeit differently, as a consequence of chain length asymmetry at the *sn*-1 and *sn*-2 positions. It is expected that partial interdigitation, at least, should also occur in the other phases ($L_c$, $P_\beta'$, and $L_\alpha$) for the asymmetric PCs in order to maximize chain–chain interactions.

The structural conclusions permit a rationalization of the thermodynamic data (Figure 3a,b). The main transition enthalpy decreases with decreasing chain length for both PC series provided that $T_m$ results from the structural phase change $P_\beta' \rightarrow L_\alpha$. The increase in transition enthalpies with decreasing acyl chain length for 18:0/12:0-PC and 18:0/10:0-PC (and perhaps 10:0/18:0-PC) is due to the interdigitated $L_\beta$* phase converting to the melted chain $L_\alpha$ phase. Finally, the total enthalpy and entropy changes for the conversion $L_c \rightarrow L_\alpha$ and have been calculated for all the PCs forming a crystalline phase and normalized by expressing them per $CH_2$ group per molecule. The results for the four members of the series 18:0/*n*:0-PC ($n$ = 18, 16, 14, or 12) are as follows: $\Delta H$ (kcal/mol) = 0.54, 0.49, 0.52, and 0.58, and $\Delta S$ (cal mol$^{-1}$ K$^{-1}$) = 1.7, 1.6, 1.6, and 2.0; while for the series *n*:0/18:0-PC ($n$ = 18, 16, 14, 12, or 10), $\Delta H$ = 0.54, 0.47, 0.40, 0.51, and 0.49, and $\Delta S$ = 1.7, 1.5, 1.3, 1.7, and 1.7, respectively. Given the possibility that we may not have generated the maximum enthalpy for the subtransition, the normalized enthalpy and entropy data suggests a similar *overall* thermodynamic change ($\Delta H \sim 0.5$ kcal/mol; $\Delta S \sim 1.7$ cal mol$^{-1}$ K$^{-1}$) for the $L_c \rightarrow L_\alpha$ conversion, although the number of phase changes involved decreases with chain length (see Figure 5a,b).

## ACKNOWLEDGMENTS

We thank Ann Tercyak, Ron Corey, and David Jackson for technical help and advice. We thank Irene Miller for help in preparing the manuscript.

## REFERENCES

Abrahamsson, S., Ställberg-Stenhagen, S., & Stenhagen, E. (1964) *Prog. Chem. Fats Other Lipids 7*, 1–157.

Abrahamsson, S., Dahlén, B., Löfgren, H., & Pascher, I. (1978) *Prog. Chem. Fats Other Lipids 16*, 125–143.

Blaurock, A. E., & McIntosh, T. J. (1986) *Biochemistry 25*, 299–305.

Boggs, J. M., & Mason, J. T. (1986) *Biochim. Biophys. Acta 863*, 231–242.

Büldt, G., Gally, H. U., Seelig, A., Seelig, J., & Zaccai, G. (1978) *Nature (London) 271*, 182–184.

Cameron, D. G., & Mantsch, H. H. (1982) *Biophys. J. 38*, 175–184.

Chang, H., & Epand, R. M. (1983) *Biochim. Biophys. Acta 728*, 319–324.

Chapman, D., Williams, R. M., & Ladbrooke, B. D. (1967) *Chem. Phys. Lipids 1*, 445–475.

Chen, S. C., & Sturtevant, J. M. (1981) *Biochemistry 20*, 713–718.

Chen, S. C., Sturtevant, J. M., & Gaffney, B. J. (1980) *Proc. Natl. Acad. Sci. U.S.A. 77*, 5060–5063.

Elder, M., Hitchcock, P., Mason, R., & Shipley, G. G. (1977) *Proc. R. Soc. London, A 354*, 157–170.

Elliott, A. J. (1965) *J. Sci. Instrum. 42*, 312–316.

Finegold, L., & Singer, M. A. (1984) *Chem. Phys. Lipids 35*, 291–297.

Finegold, L., & Singer, M. A. (1986) *Biochim. Biophys. Acta 855*, 417–420.

Franks, A. (1958) *Br. J. Appl. Phys. 9*, 349–352.

Franks, N. P. (1976) *J. Mol. Biol. 100*, 345–358.

Füldner, H. H. (1981) *Biochemistry 20*, 5707–5710.

Gupta, C. M., Radhakrishnan, R., & Khorana, H. G. (1977) *Proc. Natl. Acad. Sci. U.S.A. 74*, 4315–4319.

Hitchcock, P. B., Mason, R., Thomas, K. M., & Shipley, G. G. (1974) *Proc. Natl. Acad. Sci. U.S.A. 71*, 3036–3040.

Huang, C., & Levin, I. W. (1983) *J. Phys. Chem. 87*, 1509–1513.

Huang, C., Mason, J. T., & Levin, I. W. (1983) *Biochemistry 22*, 2775–2780.

Hui, S. W., Mason, J. T., & Huang, C. (1984) *Biochemistry 23*, 5570–5577.

Janiak, M. J., Small, D. M., & Shipley, G. G. (1976) *Biochemistry 15*, 4575–4580.

Janiak, M. J., Small, D. M., & Shipley, G. G. (1979) *J. Biol. Chem. 254*, 6068–6078.

Keough, K. M. W., & Davis, P. J. (1979) *Biochemistry 18*, 1453–1459.

Levine, Y. K., Bailey, A. I., & Wilkins, M. H. F. (1968) *Nature (London) 220*, 577–578.

Lewis, B. A., Das Gupta, S. K., & Griffin, R. G. (1984) *Biochemistry 23*, 1988–1993.

Mabrey, S., & Sturtevant, J. M. (1976) *Proc. Natl. Acad. Sci. U.S.A. 73*, 3862–3866.

Mason, J. T., Broccoli, A. V., & Huang, C. (1981a) *Anal. Biochem. 113*, 96–101.

Mason, J. T., Huang, C., & Biltonen, R. L. (1981b) *Biochemistry 20*, 6086–6092.

Mason, J. T., Huang, C., & Biltonen, R. L. (1983) *Biochemistry 22*, 2013–2018.

Mattai, J., Witzke, N. M., Bittman, R., & Shipley, G. G. (1987) *Biochemistry 26*, 623–633.

McIntosh, T. J. (1980) *Biophys. J. 29*, 237–246.

McIntosh, T. J., Simon, S. A., Ellington, J. C., Jr., & Porter, N. A. (1984) *Biochemistry 23*, 4038–4044.

Morrison, W. R., & Smith, L. M. (1964) *J. Lipid Res. 5*, 600–608.

Nagle, J. F., & Wilkinson, D. A. (1982) *Biochemistry 21*, 3817–3821.

Pearson, R. H., & Pascher, I. (1979) *Nature (London) 281*, 499–501.

Ruocco, M. J., & Shipley, G. G. (1982a) *Biochim. Biophys. Acta 684*, 59–66.

Ruocco, M. J., & Shipley, G. G. (1982b) *Biochim. Biophys. Acta 691*, 309–320.

Seddon, J. M., Harlos, K., & Marsh, D. (1983) *J. Biol. Chem. 258*, 3850–3854.

Serrallach, E. N., de Haas, G. H., & Shipley, G. G. (1984) *Biochemistry 23*, 713–720.

Stümpel, J., Nicksch, A., & Eibl, H. (1981) *Biochemistry 20*, 662–665.

Stümpel, J., Eibl, H., & Nicksch, A. (1983) *Biochim. Biophys. Acta 727*, 246–254.

Tardieu, A., Luzzati, V., & Reman, F. C. (1973) *J. Mol. Biol. 75*, 711–733.

Tümmler, B., Herrmann, U., Maass, G., & Eibl, H. (1984) *Biochemistry 23*, 4068–4074.
Wilkinson, D. A., & Nagle, J. F. (1984) *Biochemistry 23*, 1538–1541.
Wilkinson, D. A., & McIntosh, T. J. (1986) *Biochemistry 25*, 295–298.
Zaccai, G., Büldt, G., Seelig, A., & Seelig, J. (1979) *J. Mol. Biol. 134*, 693–706.

# Biosynthesis and Molecular Cloning of Sulfated Glycoprotein 2 Secreted by Rat Sertoli Cells†

Michael W. Collard and Michael D. Griswold*
*Biochemistry/Biophysics Program, Washington State University, Pullman, Washington 99164-4660*
*Received November 21, 1986; Revised Manuscript Received February 6, 1987*

ABSTRACT: Sulfated glycoprotein 2 (SGP-2) is the major protein secreted by rat Sertoli cells. Pulse–chase labeling shows that SGP-2 is synthesized as a cotranslationally glycosylated 64-kDa precursor that is modified to a negatively charged 73-kDa form before intracellular cleavage to the mature 47- and 34-kDa subunits. A plasmid cDNA library was constructed from immunopurified mRNA, and a recombinant clone containing the entire protein coding sequence of SGP-2 was isolated. The 1857-nucleotide cDNA consists of a 297-nucleotide 5′ noncoding segment, a 1341-nucleotide coding segment, and a 219-nucleotide 3′ noncoding sequence. The 5′ noncoding region contains five ATG codons followed by four short open reading frames. The derived SGP-2 sequence has a molecular weight of 51 379 and contains six potential N-glycosylation sites. Proteolytic processing sites for the preproprotein were determined by amino-terminal sequencing of the isolated SGP-2 subunits. Northern blots show a wide tissue distribution for the 2.0-kb SGP-2 message, and computer sequence analysis indicates a significant relationship between SGP-2 and human apolipoprotein A-I.

Sertoli cells are the somatic component of the seminiferous epithelium. Because of their close association with developing germinal cells and their secretory nature, Sertoli cells are thought to provide both physical and biochemical support to the process of spermatogenesis. The formation of tight-junctional complexes between adjacent Sertoli cells creates an effective "blood–testis" barrier and results in a tubular fluid composition that is defined primarily by Sertoli cell secretion products (Waites, 1977).

Analysis of proteins from cultured cells has shown that the majority of secreted protein synthesis is directed toward the production of a single sulfated glycoprotein referred to as SGP-2[1] (previously DAG protein; Kissinger et al., 1982; Sylvester et al., 1984). SGP-2 is a disulfide-linked heterodimer whose reduced subunits migrate with mobilities of 47 and 34 kDa in SDS–polyacrylamide gels. SGP-2 contains 23.7% carbohydrate, and the N-linked oligosaccharides are extensively sulfated (Griswold et al., 1986). After secretion, SGP-2 can be detected by immunofluorescence on the acrosome and distal tail portion of mature spermatozoa (Sylvester et al., 1984). Although the precise function of SGP-2 has not been defined, the binding of the protein to spermatozoa and the extent to which it is produced in Sertoli cells and epididymis suggest that SGP-2 may play a critical role in spermatogenesis.

In this paper, we present evidence that Sertoli cells synthesize SGP-2 as a single preproprotein that is then post-translationally modified and cleaved before secretion to the extracellular space. We present the nucleotide sequence of a cDNA that encodes the entire amino acid sequence of the SGP-2 precursor and examine the synthesis of SGP-2 mRNA in testis and other tissues.

## Materials and Methods

*Cell Culture and Labeling Conditions.* Sertoli cell cultures were prepared from 20-day-old rats as previously described (Dorrington & Fritz, 1975; Kissinger et al., 1982). Cells were plated onto 60-mm Falcon dishes and were maintained at 32 °C in Ham's F-12 medium supplemented with 0.1 mM dibutyryl-cAMP. The medium was changed after 2 days, and the cells were labeled after the fourth day of culture. Cells were pulsed-labeled with 200 μCi of [$^{35}$S]methionine in 0.5 mM of F-12 medium that lacked unlabeled methionine. At the end of each chase period, cells were lysed in 1.5 mL of buffer A (0.5% Triton X-100, 0.5% sodium deoxycholate, 150 mM NaCl, 50 mM Tris, pH 7.5, 5 mM EDTA, 0.5 mM phenylmethanesulfonyl fluoride) and frozen at −20 °C. The medium from the 1- and 4-h chase cells was centrifuged at 2000*g* to remove cellular debris and was frozen at −20 °C. Long-term labeling of Sertoli cell secreted proteins was achieved by incubating Sertoli cell cultures with 5 mL of

† This research was supported by National Institutes of Health Grant HD-10808 and by a grant (to M.W.C.) awarded by the Graduate School, Washington State University.
* Address correspondence to this author.

[1] Abbreviations: SGP-1, sulfated glycoprotein 1; SGP-2, sulfated glycoprotein 2; Tris, tris(hydroxymethyl)aminomethane; EDTA, ethylenediaminetetraacetic acid; DTT, dithiothreitol; cAMP, adenosine cyclic 3′,5′-phosphate; X-gal, 5-bromo-4-chloro-3-indolyl β-D-galactopyranoside; IPTG, isopropyl β-D-thiogalactopyranoside; PTH, phenylthiohydantoin; SDS, sodium dodecyl sulfate; PAGE, polyacrylamide gel electrophoresis; NBRF, National Biomedical Research Foundation; PIR, Protein Identification Resource; kDa, kilodalton(s).

0006-2960/87/0426-3297$01.50/0 